Fat-Water Interface on Susceptibility-Weighted Imaging and Gradient-Echo Imaging: Comparison of Phantoms to Intracranial Lipomas

Taha M.Mehemed[1]
Akira Yamamoto
Tomohisa Okada
Mitsunori Kanagaki
Yasutaka Fushimi
Takeshi Sawada
Kaori Togashi

OBJECTIVE. In a clinical setting, lipoma can sometime show low signal intensity on susceptibility-weighted imaging (SWI) mimicking hemorrhage. The purpose of this study was to evaluate the fat-water interface chemical-shift artifacts between SWI and T2*-weighted imaging with a phantom study and evaluate SWI in lipoma cases.

MATERIALS AND METHODS. SWI, magnitude, high-pass filtered phase, and T2*-weighted imaging of a lard-water phantom were evaluated in the in-phase, out-of phase, and standard partially out-of-phase TE settings used for clinical 3-T SWI (19.7, 20.9, and 20.0 ms, respectively) to identify the most prominent fat-water interface low signal. SWI of five cases of CNS lipoma were retrospectively evaluated by two neuroradiologists.

RESULTS. TE at 19.7 ms (in-phase) showed the minimum fat-water interface low signal in the phase-encoding direction on magnitude, high-pass filtered phase, and SWI. TE at 20.9 ms (out-of-phase) showed the maximum fat-water interface in the phase-encoding direction on magnitude, high-pass filtered phase, and SWI. TE at 20.0 ms (partially out-of-phase) showed more fat-water interface low signal on SWI than on T2*-weighted imaging, especially in the phase-encoding direction. All lipomas in the five patients showed high signal intensity with surrounding peripheral dark rim on SWI.

CONCLUSION. Fat-water interface is more prominent on the standard TE setting used for clinical SWI (20.0 ms) than that of T2*-weighted imaging and shows a characteristic surrounding peripheral low-signal-intensity rim in lipoma. Knowing the fat-water appearance on SWI is important to avoid misinterpreting intracranial lipomas as hemorrhages.

Susceptibility-weighted imaging (SWI) uses local tissue susceptibilities, such as iron deposition and blood oxygenation level–dependent (BOLD) effect, to create contrast between different tissues [1]. However, fat appearance on SWI has rarely been described [2].

Chemical-shift artifacts arise in fat-water interfaces because the fat and water protons are resonating at different frequencies from each other owing to the change of their local fields as a function of their local molecular environments, resulting in spatial misregistration of their signals. Also, because spatial positioning is assigned along the frequency-encoding direction, these artifacts tend to appear in the frequency-encoding direction; such artifacts are known as chemical-shift artifacts of the first kind.

Chemical-shift artifacts are accompanied by another artifact in gradient-echo–based imaging because of the lack of the refocusing 180° radiofrequency pulse of spin-echo sequences, resulting in a phase shift between fat and water protons. Depending on their resonance frequency due to chemical shifts, such artifacts are known as chemical-shift artifacts of the second kind [3]. At fat-water interfaces, fat and water protons go in and out of phase with one another as a function of TE and continually repeat as the TE increases. Actual TEs corresponding to the in-phase and out-of-phase status of fat and water protons are field-strength dependent. When the fat and water protons are out of phase, the signal of voxels containing the same proportion of transverse magnetization of fat and water is cancelled, producing a dark line at all fat-water interfaces. Such artifacts occur in both the frequency-encoding and phase-encoding directions [4].

In-phase and out-of-phase gradient-echo sequences have been used mainly in abdominal MRI [5] to quantify fat in the liver [6]; to differentiate between adrenal masses [7]; to identify pancreatic lymphoepithelial cysts [8]; to aid in the diagnosis of renal diseases, such as angio-

Keywords: chemical-shift artifact, fat-water interface, lipoma, susceptibility-weighted imaging

DOI:10.2214/AJR.12.10049

Received September 25, 2012; accepted after revision February 7, 2013.

[1]All authors: Department of Diagnostic Imaging and Nuclear Medicine, Graduate School of Medicine, Kyoto University, 54 Kawahara-cho, Shogoin, Sakyo-ku, Kyoto-shi, Kyoto 606-8507, Japan. Address correspondence to A. Yamamoto (yakira@kuhp.kyoto-u.ac.jp).

AJR 2013; 201:902–907

0361–803X/13/2014–902

myolipomas [9]; and to predict the likelihood of neoplastic bone marrow lesions [10]. However, the above-mentioned methods rely on the chemical-shift artifacts of the first kind, whereas this study focuses on the intravoxel chemical-shift artifacts of the second kind seen with gradient-echo imaging sequences.

T2*-weighted imaging is a gradient-echo sequence and shows such artifacts in both frequency-encoding and phase-encoding directions. On the other hand, SWI includes an extra phase component that may further enhance the appearance of the fat-water interface, especially in the phase-encoding direction. Similar chemical-shift artifacts are seen in the clinical setting of intracranial lipoma on SWI. The purpose of this study was to evaluate the fat-water interface chemical-shift artifacts between SWI and T2*-weighted imaging using a lard-water phantom model and clinical intracranial lipoma cases.

Materials and Methods

This study was approved by the local ethics committee of our institution. Because of the retrospective nature of this study, informed consent was waived.

Phantom Preparation

A lard-water phantom was prepared with the lard on the surface of the water, creating a large fat-water interface. SWI and T2*-weighted imaging were performed using a 3-T MRI scanner (Trio A Tim System, Siemens Healthcare). By use of a 32-channel head coil with a central frequency of 123.15 MHz, in-phase and out-of-phase timing were 19.7 and 20.9 ms, respectively.

The following acquisition parameters for T2*-weighted imaging in axial acquisition were used: TR/TE, 500/20.0, 19.7, and 20.9; receiver bandwidth, 199 Hz/pixel; acquisition matrix, 256 × 224; 0.39 × 0.39 × 3 mm; 1-mm gap; frequency-encoding direction in left-to-right direction; number of averages, 1; acquisition time, 1 minute 58 seconds.

The following parameters for SWI in axial acquisition were used; TR/TE, 28/20.0, 19.7, and 20.9; receiver bandwidth, 120 Hz/pixel; acquisition matrix, 320 × 230; 0.625 × 0.625 × 2 mm; no gap; frequency-encoding direction in left-to-right direction; number of averages, 1; acquisition time, 4 minutes 46 seconds.

The amounts of pixel misregistration for the SWI (120 Hz/pixel) and T2*-weighted imaging (199 Hz/pixel) were approximately 3.4 pixels and approximately 2.2 pixels, respectively.

SWI, its underlying magnitude, and high-pass filtered phase images were evaluated in the three different TE settings to identify which setting best visualized the fat-water interface as a low signal. All were compared with T2*-weighted imaging in-phase and out-of-phase fat-water interface appearances.

Gray-scale profile curve analysis was conducted for all phantom T2*-weighted imaging, SWI, high-pass filtered phase, and magnitude images acquired in the different TE settings using the plot profile function of ImageJ (National Institutes of Health) [11].

Clinical Imaging Evaluation

Five cases of CNS lipoma were selected for evaluation from the clinical imaging reporting system in our institute from 2570 SWI studies. Both CT and susceptibility-weighted images were available for all cases. SWI parameters were the same as for the phantom experiment, with a TE of 20.0 ms and acquired with phase encoding in a left-to-right direction. SWI studies were retrospectively evaluated by two neuroradiologists. Fat density on CT and a corresponding hyperintense lesion with a peripheral dark rim on SWI was considered a lipoma.

Results

Phantom Results

The in-phase (19.7 ms) and out-of-phase (20.9 ms) TE settings on T2*-weighted imaging are shown in Figure 1. Chemical-shift artifacts of the first kind in the frequency-encoding direction can be seen on the left side of the in-phase setting images of the T2*-weighted, susceptibility weighted, and magnitude images (Figs. 1, 2A, and 2C, respectively). The in-phase setting of TE at 19.7 ms showed the minimum low signal intensity between lard and water in the phase-encoding direction on magnitude and susceptibility-weighted images (Fig. 2). The out-of-phase setting of TE at 20.9 ms showed the maximum low signal intensity between lard and water in the phase-encoding direction on magnitude and susceptibility-weighted images (Fig. 3). TE at 20.0 ms showed more prominent low signal intensity on SWI than on T2*-weighted imaging (Fig. 4).

Gray-scale profile curves of the lard-water phantom on out-of-phase T2*-weighted imaging (20.9 ms) showed an increase of signal pixel values before a significant drop of signal pixel values (corresponding with the chemical-shift artifacts of the second kind) (Fig. 1B). Out-of-phase susceptibility-weighted and magnitude images (20.9 ms) showed a marked sudden low signal pixel peak (Figs. 3A and 3C) as compared with the in-phase images (Figs. 2A and 2C).

On the high-pass filtered-phase images, the fat-water interface showed an opposite biphasic pattern of appearance between the in-phase (19.7 ms) and out-of-phase (20.9 ms) TE settings, showing a bright to dark (in-phase) and a dark to bright (out-of-phase) signal from fat to water (Figs. 2B and 3B, respectively).

The partially out-of-phase susceptibility-weighted images showed the characteristic sudden low signal pixel peak occurring at the fat-water interface not seen on the T2*-weighted imaging with the same TE setting of 20 ms (Fig. 4).

Clinical Imaging Evaluation

Five lipoma cases showed high signal intensity with surrounding peripheral dark rim on SWI. Presence of fat was confirmed by CT in all cases (Fig. 5). Gray-scale profile curves of lipoma on SWI show two downward peaks of low signal pixel values (corresponding with the fat-water interface in the phase-encoding direction surrounding the lipoma) with an upward peak of higher signal pixel values (corresponding with the lipoma itself) between (Figs. 5J and 5K).

Discussion

The results of the lard-water phantom studies showed that SWI can show a more prominent low signal intensity on the fat-water interface than T2*-weighted imaging, especially in the phase-encoding direction. Clinical images of lipoma showed a prominent low-signal-intensity band surrounding the periphery of the lipoma on SWI coming from the chemical-shift artifacts of the second kind and the phase-shift contrast of the high-pass filtered-phase images between fat and water.

SWI is a 3D gradient-echo MRI technique that uses susceptibility as a source of contrast between different tissues; it includes phase postprocessing to enhance the susceptibility difference. SWI consists of an original magnitude image multiplied by a high-pass filtered-phase mask image [1]. It was first developed to visualize the venous structure of the brain on the basis of the BOLD effect by using the local susceptibility difference between intravascular deoxyhemoglobin and surrounding tissues as an intrinsic contrast mechanism to visualize the veins [1]. SWI has been used for the evaluation of hemorrhage [12], quantification of brain iron content at the basal ganglia [13], and identification of brain calcification [14].

Fat may cause a phase shift at the interface between fat and the surrounding tissue, leading to signal loss on SWI due to the above-mentioned phase-mask image effects. Chemical-shift artifacts of the second kind might also play a role in such an appearance of fat

on SWI (coming from the magnitude component). When the fat and water protons are out of phase, their signals will cancel each other, resulting in a signal void artifact in boundary pixels that contain both fat and water protons, which manifests as a sharply defined dark rim. This artifact is more commonly known as India ink artifact [15]. The phase-mask component of SWI is chosen to obtain fat roughly out of phase from water [1]. Therefore, when multiplied onto the magnitude image, the resultant susceptibility-weighted image will show the fat-water interface in the out-of-phase TE more prominently, especially in the phase-encoding direction.

Low signal intensity on SWI is known to come from local magnetic susceptibility of substances, such as iron, hemosiderin, and calcium. On the other hand, the characteristic peripheral low signal intensity surrounding lipoma on SWI comes mainly from the phase shift of the fat-water interface rather than magnetic susceptibility effects. Phase contrast is directly related to the selected TE. In the out-of-phase TE setting, the fat-water interface phase shift will be high enough to appear on the high-pass filtered-phase images and in the end will be seen as a low-signal-intensity band on the final susceptibility-weighted images.

In the case of high-pass filtered-phase images, the original phase data are high-pass filtered using a homodyne filter. Even in the calculated in-phase setting images, there might be subtle phase difference between fat and water. This subtle phase difference will be exaggerated by the homodyne filter. In the case of the out-of-phase images, the fat and water will be in opposed phase, which is π difference from in phase. Therefore, when a homodyne filter is applied, it will show the fat-water interface in an opposite direction to that seen in the calculated in-phase setting images.

On SWI, the lipoma showed hyperintensity surrounded by a low-signal-intensity band in all five cases. We believe that this characteristic appearance may be due to the partially out-of-phase (TE, 20 ms) default setting of SWI at 3-T MRI [16], which leads to a chemical shift at the lipoma-parenchyma interface in both the frequency-encoding and the phase-encoding directions. A similar appearance of lipoma on time-of-flight MR angiography source images has been reported and may mimic partially thrombosed aneurysms [17].

Lipoma appearance on conventional imaging sequences may not be problematic for neuroradiologists because on routine imaging the chemical-shift artifacts of the first kind, STIR, low-density CT attenuation, and fat-saturation techniques can be used to help distinguish fat from hemorrhage. However, the characteristic appearance of lipoma on SWI might be misinterpreted as a tumor with a hemorrhagic component. Brain tumors with a hemorrhagic component usually show peripheral low signal intensity mainly owing to susceptibility effects of blood components [18], but peripheral low signal intensity in the hemorrhagic tumor is independent from the phase-encoding or frequency-encoding directions and is not surrounding the whole tumor as in the case of lipoma. Hematomas in the brain may also resemble lipoma on SWI and present as a hyperintensity surrounded by a low-signal-intensity band, with the hyperintense part owing its appearance to the presence of methemoglobin and the surrounding dark rim to hemosiderin [19–21]. However, hematomas go through different stages and have characteristic appearances according to hemoglobin type (Fig. 6). On the other hand, the characteristic appearance of lipoma does not change owing to the aforementioned underlying mechanisms of the fat-water interface appearance on SWI. Furthermore, CT and fat-suppression MRI techniques can be valuable to differentiate between fat and blood.

For minimization of the chemical-shift artifacts, a wider receiver bandwidth is normally chosen [22]. In the case of chemical-shift artifacts of the second kind, an in-phase setting of TE will minimize such artifacts. However, in the case of lipoma, SWI has a narrower receiver bandwidth than T2*-weighted imaging, and the default partially out-of-phase setting may also contribute to the better visibility of the peripheral low signal intensity surrounding the lipoma on SWI.

Conclusion

The fat-water interface is more prominent on the standard TE setting used for clinical SWI (20.0 ms) than that of T2*-weighted imaging and shows a characteristic surrounding peripheral low-signal-intensity rim in lipoma. Knowing the fat-water appearance on SWI is important to avoid misinterpreting intracranial lipomas as hemorrhages.

Acknowledgment

We thank Katsutoshi Murata of Siemens Healthcare for his continuous help and support.

References

1. Haacke EM, Xu Y, Cheng YC, Reichenbach JR. Susceptibility weighted imaging (SWI). *Magn Reson Med* 2004; 52:612–618
2. Zaitsu Y, Terae S, Kudo K, et al. Susceptibility-weighted imaging of cerebral fat embolism. *J Comput Assist Tomogr* 2010; 34:107–112
3. Elster AD, Burdette JH. *Questions and answers in magnetic resonance imaging*, 2nd ed. St. Louis, MO: Mosby, 2001:333
4. McRobbie DW, Moore EA, Graves MJ, Prince MR. *MRI from picture to proton*. Cambridge, United Kingdom, 2003:359
5. Earls JP, Krinsky GA. Abdominal and pelvic applications of opposed-phase MR imaging. *AJR* 1997; 169:1071–1077
6. Levenson H, Greensite F, Hoefs J, et al. Fatty infiltration of the liver: quantification with phase-contrast MR imaging at 1.5 T vs biopsy. *AJR* 1991; 156:307–312
7. Tsushima Y, Ishizaka H, Matsumoto M. Adrenal masses: differentiation with chemical shift, fast low-angle shot MR imaging. *Radiology* 1993; 186:705–709
8. Kudo D, Hashimoto N, Toyoki Y, Narumi S, Hakamada K. Usefulness of in-phase and out-of-phase magnetic resonance imaging for the detection of pancreatic lymphoepithelial cyst. *Hepatogastroenterology* 2011; 58:1403–1405
9. Israel GM, Hindman N, Hecht E, Krinsky G. The use of opposed-phase chemical shift MRI in the diagnosis of renal angiomyolipomas. *AJR* 2005; 184:1868–1872
10. Disler DG, McCauley TR, Ratner LM, Kesack CD, Cooper JA. In-phase and out-of-phase MR Imaging of bone marrow: prediction of neoplasia based on the detection of coexistent fat and water. *AJR* 1997; 169:1439–1447
11. Schneider CA, Rasband WS, Eliceiri KW. NIH Image to ImageJ: 25 years of image analysis. *Nat Methods* 2012; 9:671–675
12. Wycliffe ND, Choe J, Holshouser B, Oyoyo UE, Haacke EM, Kido DK. Reliability in detection of hemorrhage in acute stroke by a new three-dimensional gradient recalled echo susceptibility-weighted imaging technique compared to computed tomography: a retrospective study. *J Magn Reson Imaging* 2004; 20:372–377
13. Haacke EM, Miao Y, Liu M, et al. Correlation of putative iron content as represented by changes in R2* and phase with age in deep gray matter of healthy adults. *J Magn Reson Imaging* 2010; 32:561–576
14. Wu Z, Mittal S, Kish K, Yu Y, Hu J, Haacke EM. Identification of calcification with MRI using susceptibility-weighted imaging: a case study. *J Magn Reson Imaging* 2009; 29:177–182
15. Bley TA, Wieben O, Francois CJ, Brittain JH, Reeder SB. Fat and water magnetic resonance im-

aging. *J Magn Reson Imaging* 2010; 31:4–18
16. Haacke EM, Mittal S, Wu Z, Neelavalli J, Cheng YC. Susceptibility-weighted imaging: technical aspects and clinical applications. Part 1. *AJNR* 2009; 30:19–30
17. Kemmling A, Noelte I, Gerigk L, Singer S, Groden C, Scharf J. A diagnostic pitfall for intracranial aneurysms in time-of-flight MR angiography: small intracranial lipomas. *AJR* 2008; 190:[web]W62–W67
18. Mittal S, Wu Z, Neelavalli J, Haacke EM. Susceptibility-weighted imaging: technical aspects and clinical applications. Part 2. *AJNR* 2009; 30:232–252
19. Gomori JM, Grossman RI. Mechanisms responsible for the MR appearance and evolution of intracranial hemorrhage. *RadioGraphics* 1988; 8:427–440
20. Schrag M, McAuley G, Pomakian J, et al. Correlation of hypointensities in susceptibility-weighted images to tissue histology in dementia patients with cerebral amyloid angiopathy: a postmortem MRI study. *Acta Neuropathol* 2010; 119:291–302
21. Sehgal V, Delproposto Z, Haddar D, et al. Susceptibility-weighted imaging to visualize blood products and improve tumor contrast in the study of brain masses. *J Magn Reson Imaging* 2006; 24: 41–51
22. Parizel PM, van Hasselt BA, van den Hauwe L, Van Goethem JW, De Schepper AM. Understanding chemical shift induced boundary artefacts as a function of field strength: influence of imaging parameters (bandwidth, field-of-view, and matrix size). *Eur J Radiol* 1994; 18:158–164

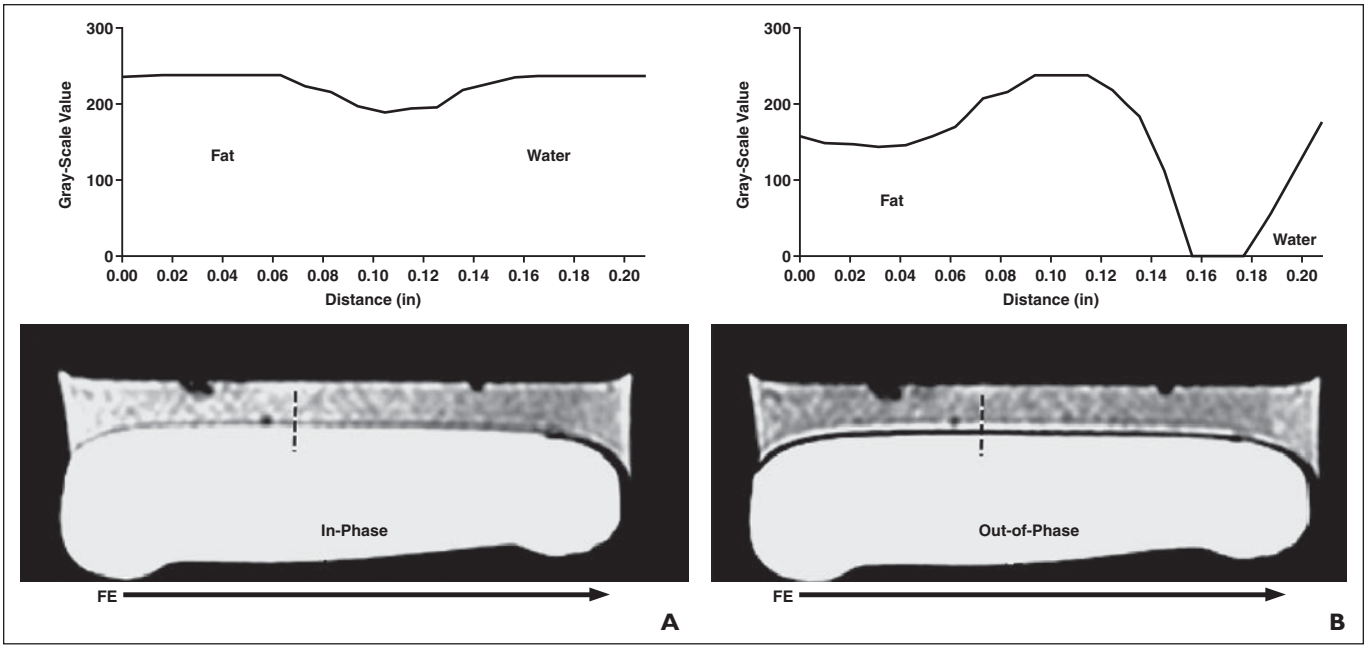

Fig. 1—Chemical-shift artifact.
A and **B,** T2*-weighted images with TE of 19.7 ms (**A**) and 20.9 ms (**B**) of lard-water phantom show fat-water interface appearance, with TE of 20.9 ms (out-of-phase) showing clearest chemical-shift artifact and TE of 19.7 ms showing least apparent chemical-shift artifact. Gray-scale profile curves are shown on top of each image. Dashed lines correspond with distance scale depicted in gray-scale profile curves. FE = frequency-encoding direction.

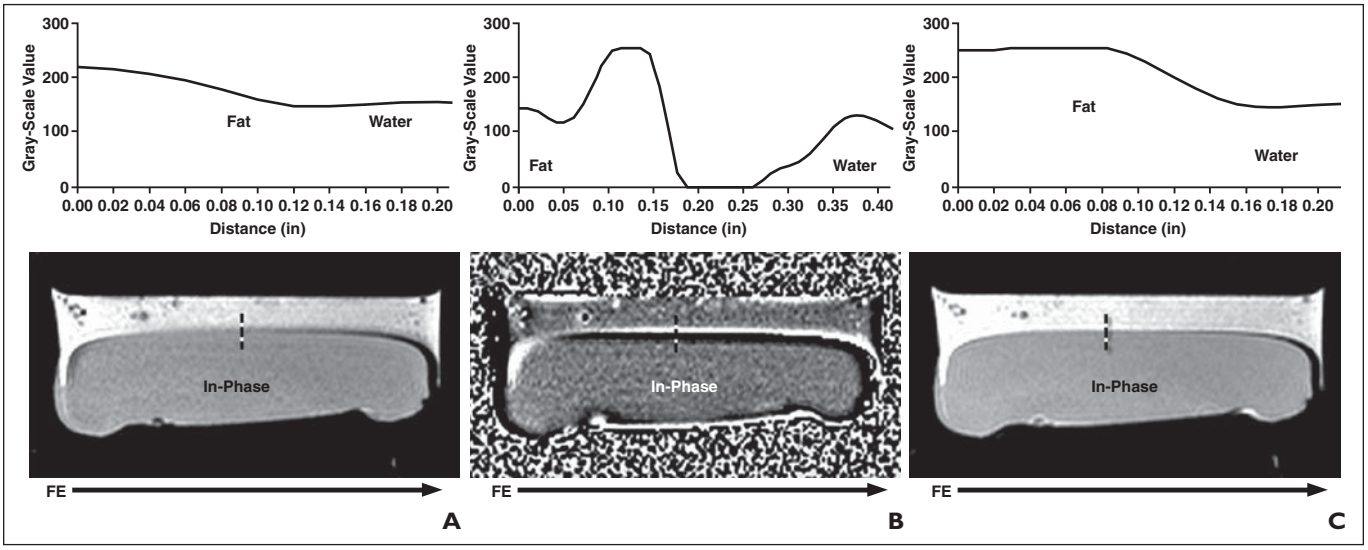

Fig. 2—Minimum appearance of fat-water interface.
A–C, Susceptibility-weighted (**A**), high-pass filtered phase (**B**), and magnitude (**C**) images of lard-water phantom, with TE setting of 19.7 ms (in-phase), show minimum appearance of fat-water interface. Gray-scale profile curves are shown on top of each image. Dashed lines correspond with distance scale depicted in gray-scale profile curves. FE = frequency-encoding direction.

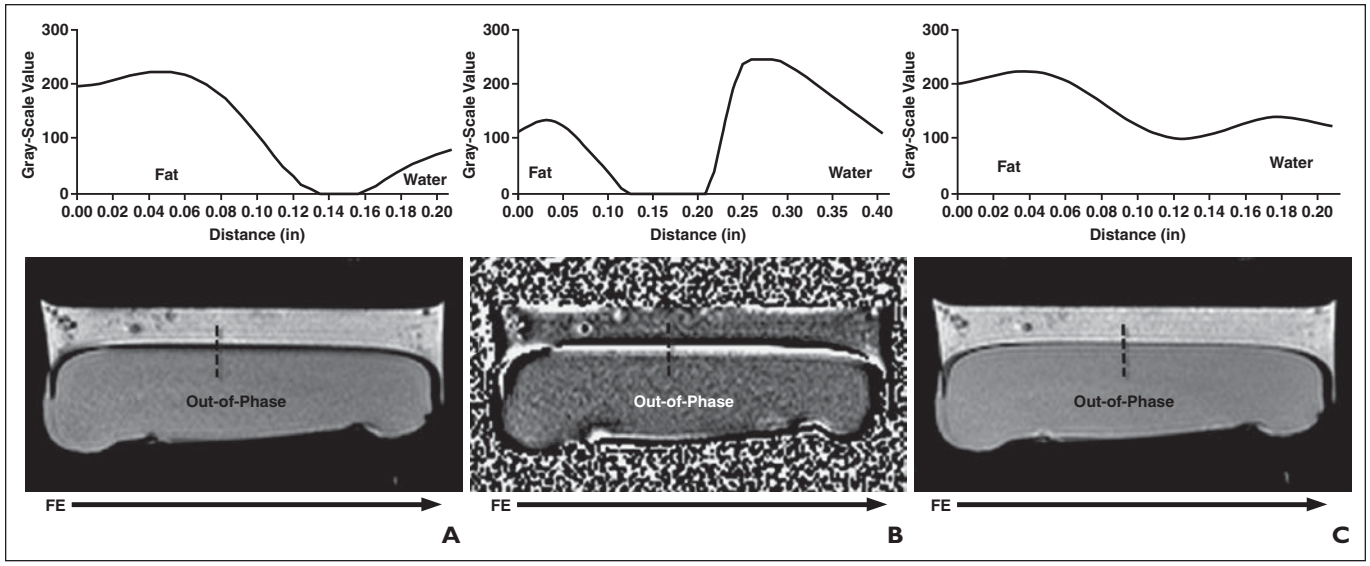

Fig. 3—Maximum appearance of fat-water interface.
A–C, Susceptibility-weighted (**A**), high-pass filtered phase (**B**), and magnitude (**C**) images of lard-water phantom, with TE setting of 20.9 ms (out-of-phase), showing maximum appearance of fat-water interface. Gray-scale profile curves are shown on top of each image. Dashed lines correspond with distance scale depicted in gray-scale profile curves. FE = frequency-encoding direction.

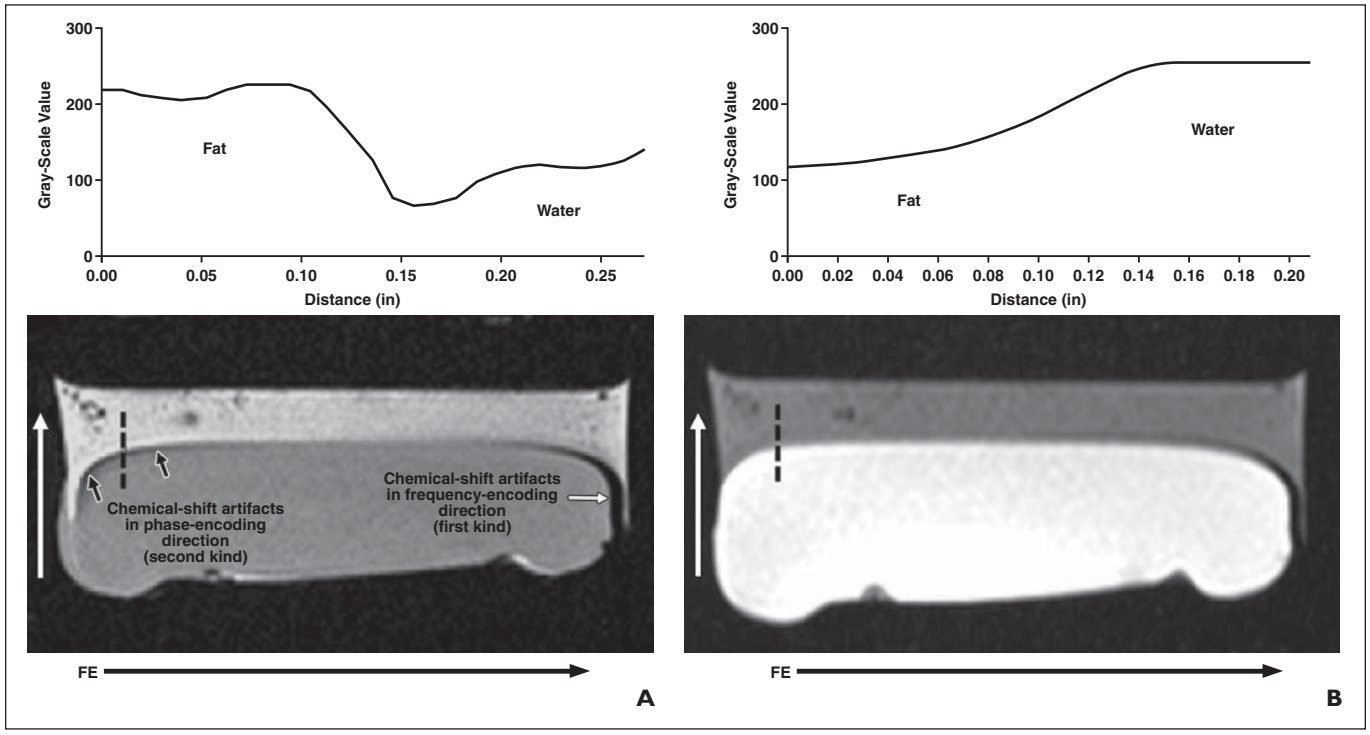

Fig. 4—Fat-water interface.
A and **B,** Susceptibility-weighted (**A**) and T2*-weighted (**B**) images of lard-water phantom with TE setting of 20 ms (partially out-of-phase susceptibility-weighted imaging [SWI] default setting) show more prominent appearance of fat-water interface on SWI than T2*-weighted imaging. Gray-scale profile curves are shown on top of each image. Small black arrows (**A**) indicate fat-water interface visualized in SWI and not on T2*-weighted imaging. Vertical white arrows indicate phase-encoding direction. Dashed lines correspond with distance scale depicted in gray-scale profile curves. FE = frequency-encoding direction.

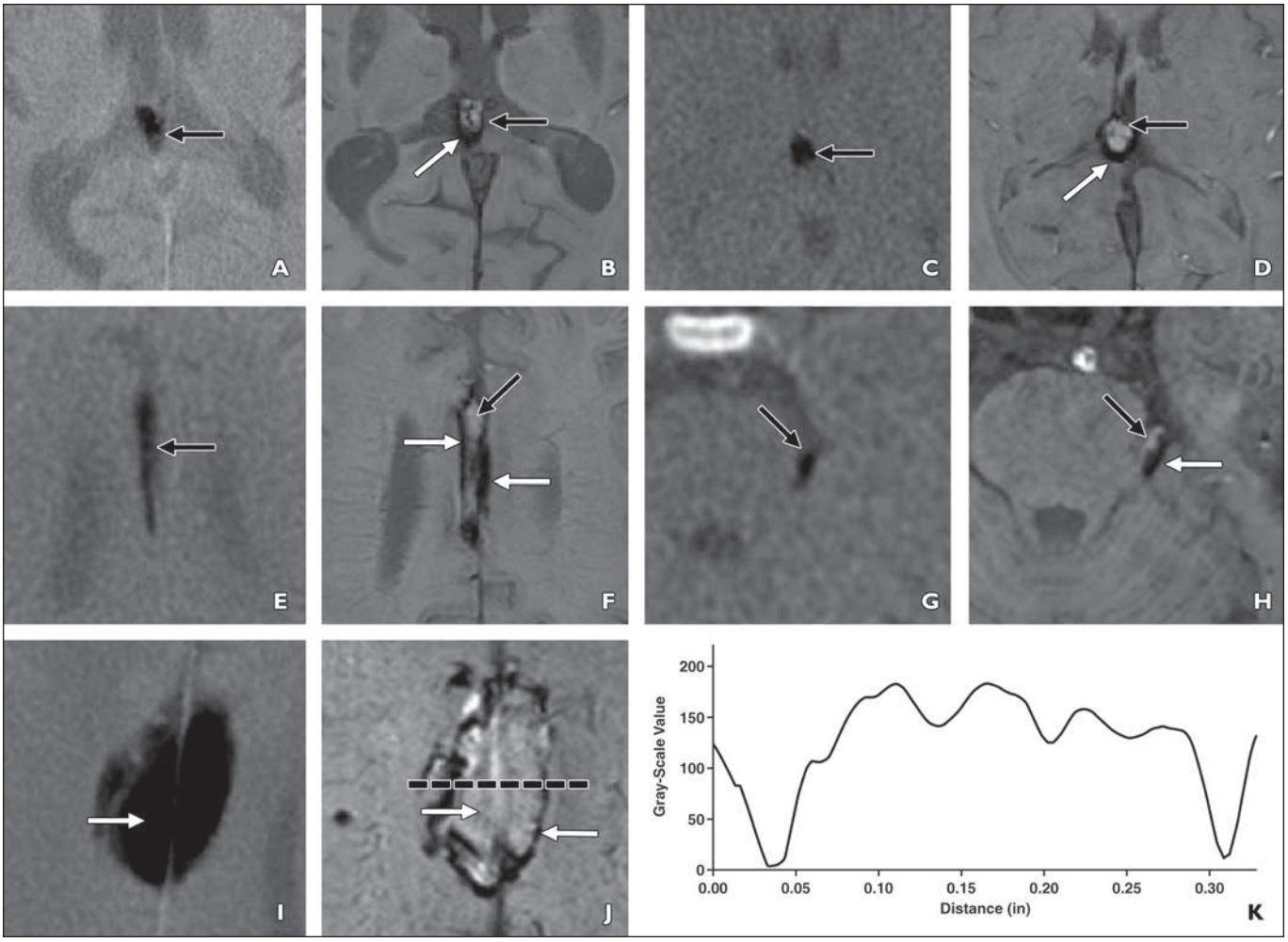

Fig. 5—Five patients with lipoma.
A–K, Susceptibility-weighted and corresponding CT images of five patients with lipoma: 80-year-old man (**A** and **B**), 15-year-old boy (**C** and **D**), 59-year-old woman (**E** and **F**), 3-year-old boy (**G** and **H**), and 68-year-old man (**I** and **J**). Black arrows show lipoma on CT and susceptibility-weighted images, and white arrows show chemical-shift artifact resultant from fat-water interface on susceptibility-weighted images). Magnified lipoma on SWI (**J**) and corresponding gray-scale profile curve (**K**) are shown. Dashed line corresponds with distance scale depicted in gray-scale profile curve.

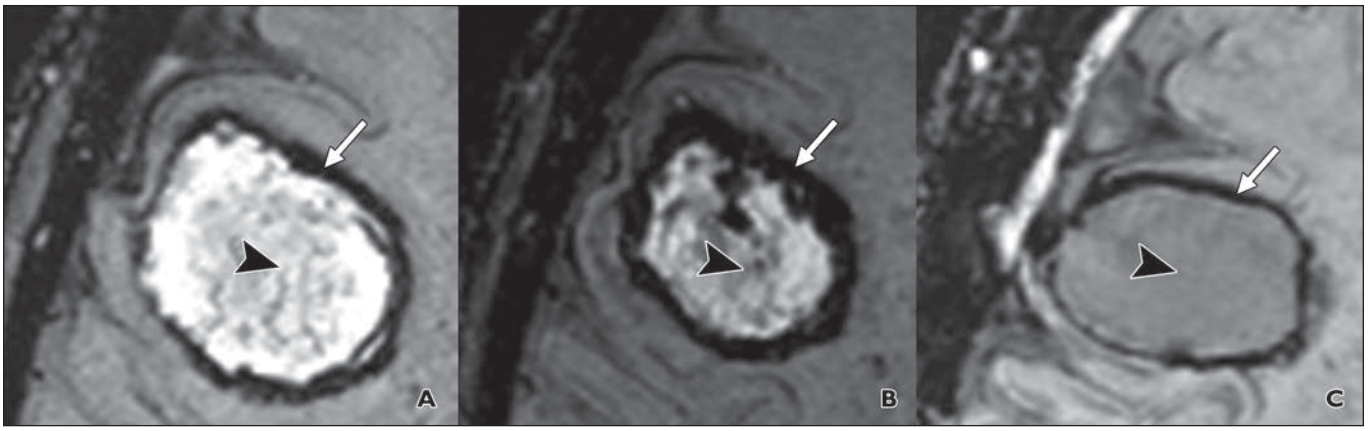

Fig. 6—49-year-old man.
A–C, Serial susceptibility-weighted images show temporal evolution of chronic intracranial hematoma. Note intrahematoma signal change from high signal (*arrowheads*) representing phase of increased RBC destruction leading to disappearance of deoxyhemoglobin and methemoglobin susceptibility effects and peripheral hypointense rim (*arrows*) representing deposition of hemosiderin and ferritin. In later stages, intrahematoma signal changes to low signal because of increased hemosiderin and ferritin susceptibility effects (**C**).